Computer-Aided Placement of Deep Brain Stimulators: From Planning to Intraoperative Guidance

Pierre-François D'Haese, *Member, IEEE*, Ebru Cetinkaya, Peter E. Konrad, Chris Kao, and Benoit M. Dawant*, *Senior Member, IEEE*

***Abstract*—In current practice, optimal placement of deep-brain stimulators (DBSs) used to treat movement disorders in patients with Parkinson's disease and essential tremor is an iterative procedure. A target is chosen preoperatively based on anatomical landmarks identified on magnetic resonance images. This point is used as an initial position that is refined intraoperatively using both microelectrode recordings and macrostimulation. In this paper, we report on our current progress toward developing a system for the computer-assisted preoperative selection of target points and for the intraoperative adjustment of these points. The system consists of a deformable atlas of optimal target points that can be used to select automatically the preoperative target, of an electrophysiological atlas, and of an intraoperative interface. Results we have obtained show that automatic prediction of target points is an achievable goal. Our results also indicate that electrophysiological information could be used to resolve structures not visible in anatomic images, thus improving both preoperative and intraoperative guidance. Our intraoperative system has reached the stage of a working prototype and we compare targeting accuracy as well as the number of paths needed to reach the targets with our system and with the method in current clinical use.**

***Index Terms*—Atlas-based methods, computer-assisted surgery, deep brain stimulation, electrophysiological atlas, nonrigid registration.**

I. Background

SINCE its first FDA approval in 1998 deep-brain stimulation (DBS) has gained significant popularity in the treatment of movement disorders [1], [2]. The therapy has significant applications in the treatment of tremor, rigidity, and drug induced side effects in patients with Parkinson's disease and essential tremor. This procedure, which necessitates placing electrodes within targets ranging from 4–12 mm in diameter, requires stereotactic neurosurgical methodology. Typically, the process of implantation of a DBS electrode follows a step-wise progression of: 1) initial estimation of target localization based on imaged anatomical landmarks; 2) intraoperative microanatomical mapping of key features associated with the intended target of interest; 3) adjustment of the final target of implantation by appropriate shifts in three dimensional space; and 4) implantation of a quadripolar electrode with contacts located surrounding the final desired target. These steps are required because some of the surgical targets of interest involve deep brain nuclei such as the Vim (Ventral intermediate nucleus), the subthalamic nucleus (STN), or the Ventrocaudalis nucleus that are poorly visible in current imaging modalities. In the case of the STN, pulse sequences have been proposed in recent years to improve visualization but even with these sequences, the exact boundary of the structure is not always visible [3], [4]. Preoperatively, the location of these targets is thus typically inferred approximately from the position of adjacent structures that are visible in the images (e.g., from the anterior and posterior commisures or from the substantia niagra and the descending internal capsule [4]). This approximate location is then refined intraoperatively. The intraoperative adjustment of the target point is based on the surgical team's (at our institution, this team involves a neurosurgeon, a neurophysiologist, and a neurologist) interpretation of electrophysiological recordings and responses to stimulations. Anecdotal evidence based on conversations with the surgical team and observations of the procedure suggest that intraoperative electrode adjustment involves: 1) matching a set of input data (e.g., loss of rigidity, firing rate, severity of side effects, stimulation voltage, etc.) with electrophysiological landmarks that can be related to the target of interest; 2) planning and execution of a displacement from the current position to the desired one. For instance, as a result of test stimulations applied through a trajectory, the clinical team may observe that unacceptable double vision occurs along with mild symptomatic relief of rigidity. The interpretation of this information would be that the trajectory is too medial. The difficult anatomical question at this point is: in this particular patient how far lateral does the trajectory need to be moved, e.g., 1, 2, or 3 mm. Because of anatomical differences between patients, this question is difficult to answer. It could, however, be more easily answered if the current position could be mapped onto an atlas, the displacement determined in the

Manuscript received April 15, 2005; revised July 20, 2005. The work of P.-F. D'Haese was supported in part by the FRIA, the FNRS (Belgian Science Foundation), and the Walloon Region through the MERCATOR project. Parts of this work were presented at the MICCAI 2004 conference. The Associate Editor responsible for coordinating the review of this paper and recommending its publication was K. Cleary. *Asterisk indicates corresponding author.*

P.-F. D'Haese is with the Department of Electrical Engineering, Catholic University of Louvain (UCL), Louvain, Belgium and also with the Department of Electrical Engineering and Computer Science, Vanderbilt University, Nashville, TN 37235 USA (e-mail: pierre-francois.dhaese@vanderbilt.edu).

E. Cetinkaya is with the de Department of Electrical Engineering and Computer Science, Vanderbilt University, Nashville, TN 37235 USA.

P. E. Konrad is with the Department of Neurological Surgery, Vanderbilt University, Nashville, TN 37235 USA.

C. Kao is with the Department of Neurological Surgery, Vanderbilt University, Nashville, TN 37235 USA. He is also with the Sentient Medical Systems, Cockeysville, MD 21030 USA.

*B. M. Dawant is with the Department of Electrical Engineering and Computer Science, Vanderbilt University, Nashville, TN 37235 USA (e-mail: benoit.dawant@vanderbilt.edu).

Digital Object Identifier 10.1109/TMI.2005.856752

atlas, and this displacement mapped back onto the patient. Doing so requires several key ingredients: 1) accurate algorithms to register patients and atlases; 2) populating the atlases with information that permits the labeling of structures and substructures based on their electrophysiological signatures; and 3) mapping electrophysiological signals to landmarks in the atlas. This paper describes our efforts toward developing a guidance system for the automatic presurgical selection of the target of interest and the guidance of the intraoperative adjustment. We note that others have proposed the creation of an electrophysiological atlas [5], [6] for computer-assisted planning and guidance of deep brain stereotactic procedures but to the best of our knowledge, ours is the first one that has been used for the prediction of target points. It is also the first one that includes information derived from the microelectrode recordings.

II. Method

A. Data

With IRB approval (Vanderbilt University IRB #010 809), a set of computed tomography (CT) and magnetic resonance imaging (MRI) volumes are acquired preoperatively for each patient. These are acquired with the patient anesthetized and head taped to the table to minimize motion. Typical CT images are acquired at $\mathrm{kvp} = 120\ \mathrm{V}$, $\mathrm{exposure} = 350\ \mathrm{mas}$, 512×512 voxels ranging in size from 0.49 to 0.62 mm, and slice thickness from 1 to 2 mm; MR images acquired with a 1.5 T GE Signa scanner are 3D SPGR volumes, TR: 12.2 ms, TE: 2.4 ms, flip angle 20.0°, number of averages 1.0, dimension $256 \times 256 \times 124$ voxels, typical voxel dimensions $0.85 \times 0.85 \times 1.3\ \mathrm{mm}^3$. Since March 2004 (i.e., patients on which our method has been tested prospectively) a second T2-weighted MR sequence (2D Turbo Spin Echo TR: 4000 ms, TE: 39 ms, flip angle 90.0 degrees, number of averages 2.0, typical volume dimension $256{*}256{*}112$ voxels, typical voxel dimensions $1 \times 1 \times 1.5\ \mathrm{mm}^3$ that improves contrast in the area of the STN has been acquired. For the work described in this paper, the atlas has been created with 21 subjects. It was subsequently frozen, and used prospectively on six subjects.

B. Manual Preoperative Selection of Target Points

Preoperative target identification is performed by the functional neurosurgeon (P.E.K.) and is based on an identification of the anterior and posterior commissure (AC-PC) location and arriving at 4 mm posterior, 12 mm lateral, and 3–4 mm inferior to the midcommissural point for STN, which corresponds to stereotactic coordinates published in the literature for the center of the STN's motor territory [3]. Small adjustments to these target points are then made based on the width of the third ventricle and other anatomical asymmetries noted on the MRI scans to attempt to compensate for individual variation in nuclear locations [3].

C. Intraoperative Placement and Guidance System

Traditional methodology for carrying out the stepwise target localization procedure followed for DBS implantation requires an externally attached rigid fixture, called a "stereotactic frame" that encompasses the patient's head and upon which micro-manipulating equipment can be mounted and maneuvered with sub-millimetric precision. Recently, the FDA approved a miniature stereotactic frame, the StarFix microTargeting Platform (501(K), Number K003776, Feb. 23, 2001, FHC, INC; Bowdoinham, ME). This device, which is used at our institution, presents several advantages: 1) Separation of the phase of the procedure that includes image acquisition and target planning from the actual day of the surgery. This allows for CT and MR images to be acquired under anesthesia and thereby reduce motion artifacts on the resultant images. 2) Patients are not tethered to the bed since the platform is small enough not to require stabilization thus reducing patient discomfort during the procedure. 3) The platform permits simultaneous bilateral implantation, which is not possible with traditional frames.

The FDA clearance of this platform was based on manufacturing standards that demonstrated submillimetric targeting accuracy on phantom experiments. More recently, [7] a study that evaluates the accuracy of this platform in a clinical setting has been reported. This study compares the distance between the position observed in postoperative CT images and the position calculated relative to the platform from the preoperative image. This error is called the electrode placement error (EPE). The study, conducted on 20 implantations reports a root mean square (RMS) EPE inferior to 2.9 mm, which compares favorably to previously published values of 4.1 mm and 3.4 mm for a standard Leksell stereotactic frame (Elekta Instruments, Stockholm, Sweden) [3], [8]. One source of EPE in the data set used to conduct the study reported in [7] is the way the final electrode was anchored to the skull, which could introduce a displacement along the track direction. Since then, we have improved the anchoring method and repeated the assessment for 16 implantations. With the improved anchoring, RMS EPE was reduced to 2.06 mm. The platform mounted on a skull is shown in Fig. 1(a). A top view of the guide through which the electrodes are inserted is shown in Fig. 1(b). The five holes in this guide permit the insertion of the electrodes along five parallel tracks. During surgery, a micropositioning drive (microTargeting drive system, FHC Inc., Bowdoinham, ME) is mounted on the platform [Fig. 1(c)]. Recording and stimulating leads are then inserted through the guiding tubes. The StarFix platform is designed based on the CT images (geometric distortions that affect the markers in MR images reduce platform accuracy when this modality is used) and its design is such that the preoperative target is located on the central track. The depth of the electrode is read from the micropositioning device and converted into x, y, and z CT coordinates.

D. Rigid and Nonrigid Registration Algorithms

Two types of registrations algorithms are needed to process our data: rigid and nonrigid. The rigid registration algorithm is required to register MR and CT volumes of the same patient. This is necessary because, as mentioned above, the intraoperative position of the recording and stimulating electrodes provided by the micropositioning drive are in CT coordinates. The algorithm we have used to register MR and CT images of the same patient is an independent implementation of a standard mutual information (MI)-based algorithm [9]. This algorithm has been validated using the data sets provided by the Retrospective Image Registration Evaluation Project (RIRE: http://www.vuse.vanderbilt.edu/~image/registration/).

(a) (b) (c)

Fig. 1. STarFix platform: (a) mounted on phantom skull. (b) with guide-tubes in place. The central tube guide is aimed at the initially chosen target. The other tubes, each at a distance of 2 mm from the central tube are used for lateral adjustments. The cluster of five tubes can itself be shifted radially by 3 mm (not shown), (c) with micropositioning device mounted on the platform during surgery.

The ground truth transformations used to validate registration algorithms in this project have been obtained at Vanderbilt with bone-implanted marker and are kept confidential from other sites. One of the rules that has been established when this project was initiated is that any investigator affiliated with Vanderbilt could not have his/her registration algorithm evaluated officially. However, our algorithm has been evaluated unofficially (i.e., results of the validation have not been posted on the project website) on the same datasets that have been used to validate the other algorithms. The median errors obtained when registering CT to T1 and T2 rectified MR images with our algorithm were 0.99 mm and 0.97 mm, respectively. At the time of writing, 72 MI-based algorithms have been evaluated by the RIRE project on the CT to T1 rectified MR images and 65 on the CT to T2 rectified MR images. We have computed the median error for each of these methods and then computed the averages. These are 2.83 mm and 3.45 mm for the T1 and T2 sets, respectively. The medians of the medians are 0.87 mm and 0.92 mm. The results obtained with our algorithm are thus comparable to other MI-based rigid body registration algorithms that have been evaluated officially. We have evaluated our algorithm on rectified MR images because geometric distortions in MR images affect the bone implanted markers, thus reducing the achievable accuracy obtained with this technique.

Nonrigid registration is required to register patient data to an atlas and vice-versa. In this study, nonrigid registration is always performed on MR image volumes using an algorithm we have proposed recently [10]. Briefly, this algorithm computes a deformation field that is modeled as a linear combination of radial basis functions with finite support. This results in a transformation with several thousands of degrees of freedom. The similarity measure we use is the Mutual Information between the images. We also compute simultaneously two transformations (one from the atlas to the subject and the other from the subject to the atlas) that are constrained to be inverses of each other.

Validation of nonrigid registration algorithms is an open-ended problem but we have evaluated our algorithm in several ways. In [10], we conduct a validation study in which automatic contours obtained by deforming an atlas using our algorithm and manual contours were compared. This study showed a very good agreement between manual and automatic contours for the whole head, the brain stem, and the eyes. We have also evaluated the accuracy of our registration algorithm in the following way.

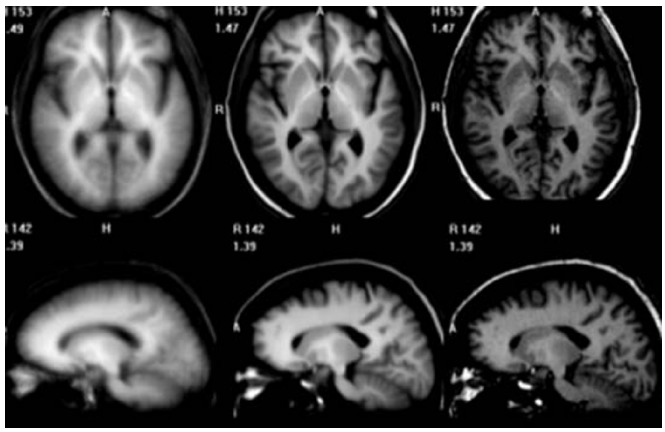

Fig. 2. Average of 39 volumes registered to the same reference (right) using nine DOFs (left panels) and nonrigid (middle panels) registration algorithms.

Among 40 MR brain image volumes, we have chosen one as a reference. We have then registered the 39 remaining volumes to the reference volume, first with a nine degrees of freedom (DOFs) transformation, then with our nonrigid registration algorithm. The 9 DOFs registration algorithm is the same as the one we use for rigid body registration but we add three degrees of freedom (anisotropic scaling). After registration, we average all the volumes. Fig. 2 shows the results we have obtained. The left panels are a transverse and a sagittal view of the average volume after registration with a nine DOFs transformation. The middle panels show the same but after nonrigid registration. The right panels are the corresponding slices in the reference volume to which all the others have been registered. The blurriness visible in the left image shows that a 9 DOFs transformation cannot compensate for large anatomical differences between volumes, which results in approximate matching of homologous structures and blurring of the boundaries. Blurriness has been greatly reduced in the images displayed in the middle panels. In fact, contrast is better in the average obtained after nonrigid registration than in the reference volume because averaging has improved the signal-to-noise ratio. These results strongly suggest that our algorithms are able to register accurately MR images pertaining to different subjects, at least for structures that are visible in these images. As discussed earlier, the visibility of the structures targeted by DBS procedures is poor. It is thus difficult to assess directly the accuracy of our

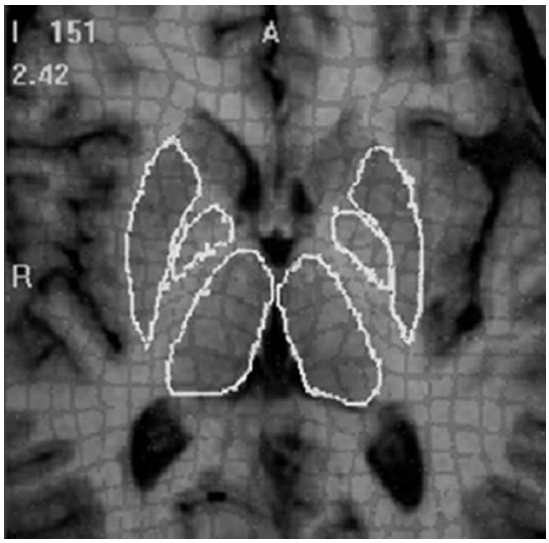

Fig. 3. One subject registered to the atlas; the contours are the outline of the globus palladus, the putamen, and the thalamus delineated in the atlas. The images also shows the smoothness and regularity of the deformation field by means of a deformed grid.

registration algorithm for these structures. An indirect way to assess this accuracy is to look at the deformation field produced by our registration algorithms and determine if it is smooth and regular over homogeneous regions or regions with poor contrast. Fig. 3 shows typical results we have obtained. The figure shows one subject registered to the atlas. The contours are the outline of the globus palladus, the putamen, and the thalamus delineated in the atlas. The regularity of the deformation field is demonstrated by means of a superimposed deformed grid. It shows a regular grid (i.e., orthogonal lines) defined in the patient volume that has been deformed with the computed deformation field. The resulting deformed gird is superimposed on the deformed patient's volume, showing the regularity of our transformation. Ultimately, however, validation of nonrigid registration algorithms is task dependent. In our results section, we show that our algorithms can cluster target points selected intraoperatively onto the atlas within the STN and that our method can be used to predict target points preoperatively.

E. Intraoperative Electrophysiological Recordings and Processing of These Recordings

Micro-electrical signals have been recorded intraoperatively for 13 patients and saved using the dual channel LeadPoint system from Medtronic Neurological. These signals were recorded along the electrode path starting 10 mm above the preoperative target point and ending 5 mm below. Signals were recorded every 0.5 mm for 10 s, and sampled at 22 kHz. After the procedure, the digitized signals and the position at which these signals have been acquired, which is provided intraoperatively by the micropositioning device (see Section II-C), are downloaded from the LeadPoint system and stored on file for further processing. At the time of writing, over 2700 signal epochs have been used. Intraoperative electrophysiological signals are often categorized in terms of firing rate (FR) that measures tonic activity and indices that measures phasic activity, including the burst index (BI), pause ratio (PR), pause index (PI), or interspike

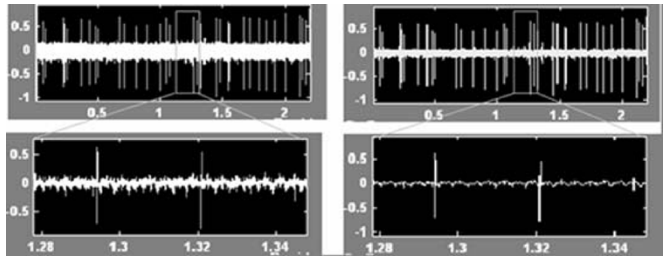

Fig. 4. Results obtained with the wavelet de-noising algorithm. The top-left window displays the nonprocessed signal, the top-right window shows the de-noised signal. Zoomed view of the original signal and the de-noised signal are displayed on the bottom-left and on the bottom right, respectively.

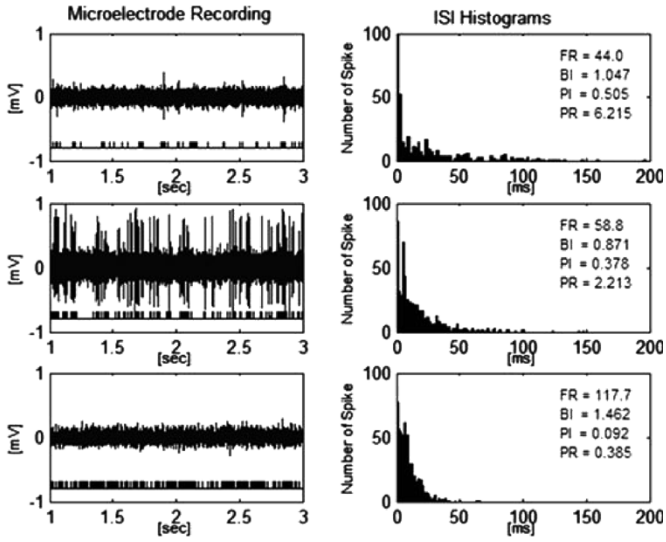

Fig. 5. Examples of raw and processed signals, and values for features extracted from these signals.

interval histogram (ISI) [11]. In this work, we have implemented a series of signal processing algorithms that permit us to compute the same features. We start with the raw signals, which we denoise using a wavelet-based denoising algorithm. More specifically, we decompose the signal into five levels using a Daubechies-8 mother wavelet, we threshold wavelet coefficients using a hard-thresholding approach [12], [13] and we reconstruct the signals. Fig. 4 shows an example of the results obtained with this algorithm. Once the signals are denoised, spikes are detected using a technique that is based on a nonlinear energy operator (NEO) introduced by Maragos [14] to estimate the instantaneous frequency and amplitude of sinusoidal signals. It was later shown that the output of this operator yields the instantaneous energy of the high-pass version of the signal and that it could be used as a robust transient detector [15]. As proposed by Mukhopadhyay [15] spikes are detected by thresholding this output signals. The threshold is chosen to be a scaled version of the mean of the output signal. In this work, the value of the threshold has been set to 6. This value was found experimentally to lead to a good compromise between missing spikes and generating false alarms.

Once spikes are detected, the aforementioned features can be computed. Fig. 5 shows some of the results we have generated. From top to bottom the three signals are epochs that have been recorded along an electrode path. The first row corresponds to a position above the STN, the middle one is in the middle of

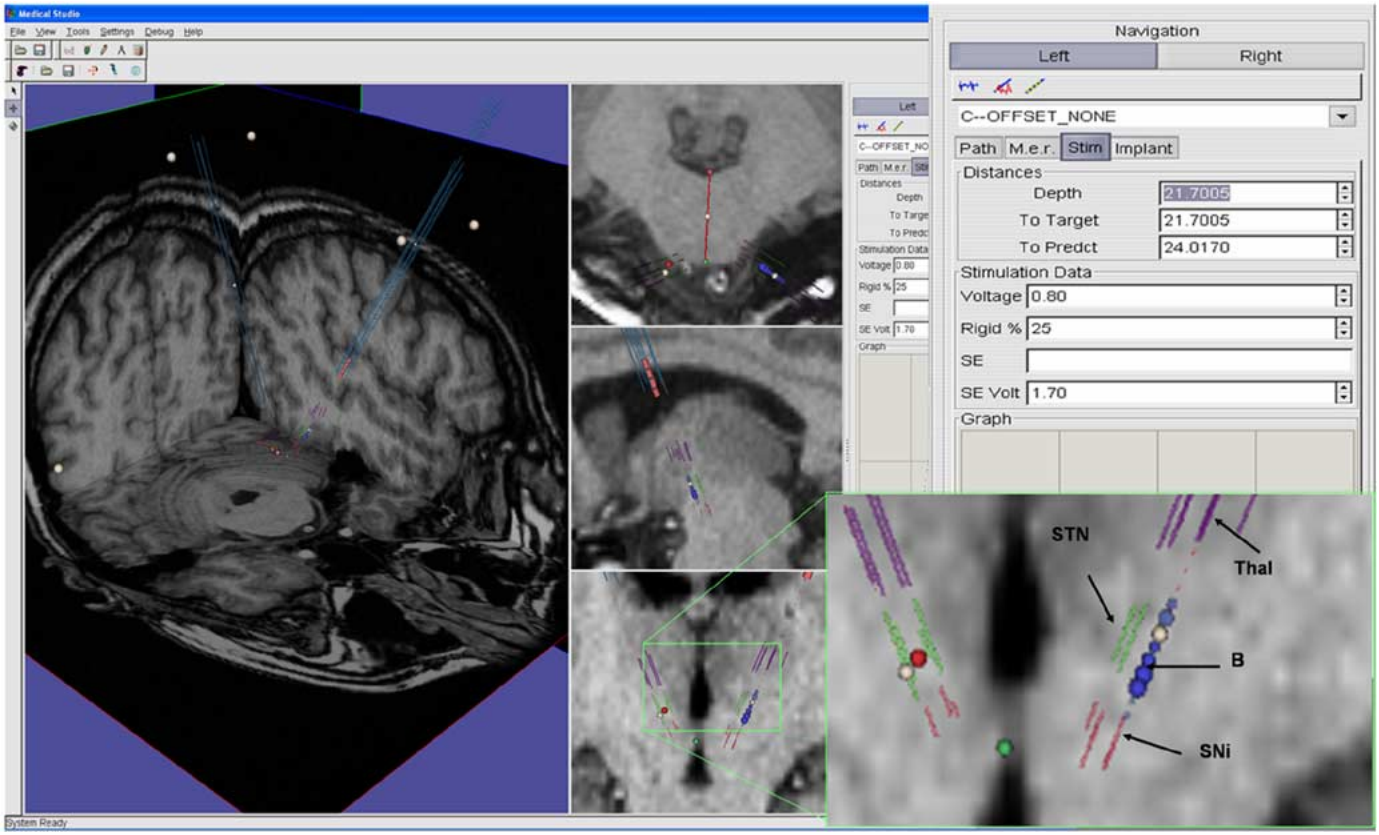

Fig. 6. Snapshot of the user interface we have developed to acquire and visualize information intraoperatively. In the magnified part, parallel lines represent intraoperative trajectories. Labels based on intraoperative interpretation of electrophysiological signals: Purple=Thalamus; Green=STN; Red=Substantia Nigra. Blue spheres (label B on figure) are used to visualize effect of stimulation on disappearance of symptoms and appearance of side effects.

the STN, and the bottom one below the STN. The left panels show the raw signal as well as the spikes we have extracted from these signals (black spike trains on the bottom of the left panel). The right panels show the interspike interval (ISI) histogram as well as the value for the features we have computed. Once features have been extracted, their values can be color-coded and displayed in the atlas.

F. Intraoperative System

We have developed an intraoperative system that permits both the capture of intraoperative information and the display of information extracted from the atlas and tailored to the patient. Fig. 6 presents a snapshot of our current user interface. The magnified panel with the colored lines shows the visualization scheme we have developed with the surgical team to display information acquired intraoperatively. The parallel lines show electrode trajectories for a particular patient. The colored dots along these trajectories indicate the label the surgical team has assigned to the position (purple=thalamus, green=STN, red=substantia nigra). The blue spheres (label B on the figure) are used to visualize the efficacy of the stimulation at a point along the trajectory. We use two parameters to visualize this information: the diameter of the sphere and the transparency of the color. The diameter is proportional to $\mathrm{Veff} = (\mathrm{Vside} - \mathrm{Vsym})$ with Vsym the voltage required to alleviate the symptoms and Vside the voltage at which side effects begin to appear. The larger Veff the better the position. Opacity is proportional to the loss of rigidity. Thus, a very good position appears on our display as a large and opaque blue sphere. The dialog box is used intraoperatively by the surgical team to enter the information that cannot be acquired automatically. Currently this includes the voltage applied to the stimulating electrode, the presence or absence of side effects, and the location of these side effects (e.g., left leg, right arm, etc.); when side effects are observed, the surgical team can qualitatively assess and enter their magnitude. The system permits entering an assessment on the loss of rigidity produced by the stimulating electrode, or the label of the nucleus in which the electrode is located. All this information is entered in a relational database. The interface also shows the depth of the electrode as well as its distance from the target selected preoperatively by the surgeons and the distance from the target predicted by our system.

III. Results

A. Registration Accuracy and Creation of an Atlas of Target Points

As discussed earlier, validation of nonrigid registration algorithms is a notoriously difficult problem because of the lack of "gold standards." For certain applications such as atlas-based segmentation tasks, validation can be achieved by comparing contours or volumes of structures with those obtained manually. Even though a gold standard is typically not available for these tasks, techniques have been proposed recently to estimate it

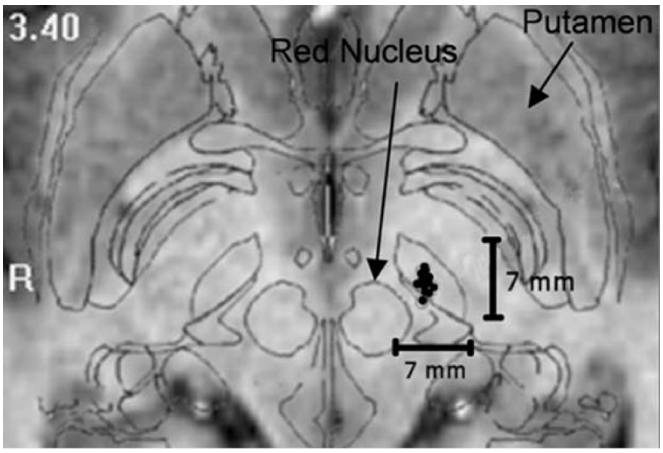

(a)

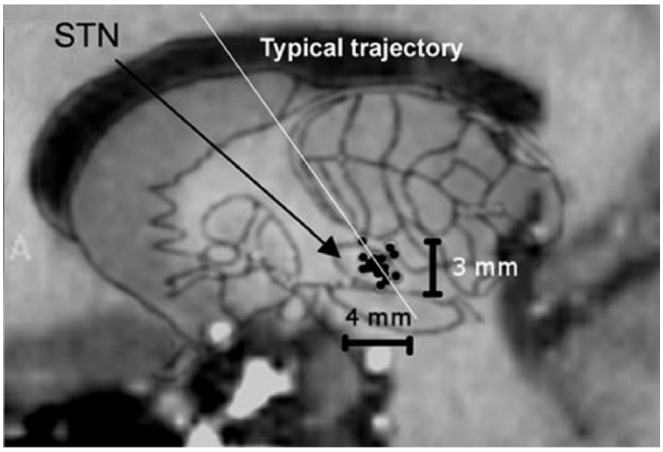

(b)

Fig. 7. DBS positions selected intraoperatively mapped onto the atlas. Points are projected onto the transverse (a) and sagittal (b) slices passing through the centroid of the clusters.

from several manual delineations [16]. For our application, such ground truth cannot be obtained and we can only assess the accuracy of our entire system and its adequacy for our long-term objectives indirectly. To do so, we make two assumptions. 1) Although it is unknown whether or not the stimulator should be placed at the exact same anatomic location (there is no one-to-one mapping between anatomy and function) for every patient, these positions will not be very far apart in patients with the same type of disease. 2) During the procedure, the surgical team is able to place the stimulator at the optimal position even if the point chosen preoperatively was suboptimal (this is done intraoperatively using microelectrode recordings and responses to stimulations). With these assumptions, final target points chosen intraoperatively should be mapped approximately onto the same anatomic location in the atlas.

In this paper, we have chosen one of the subjects as the reference, which we call the atlas, and we have registered all the other volumes to it. We have then projected every final target point chosen intraoperatively onto the atlas, thus creating two clouds of points (one for the left and the other for the right STN). Fig. 7 shows the results we have obtained on the right side. In this figure, we show both our points and contours of anatomic

TABLE I

Distance from centroids for STN (in mm)								
	Left				Right			
	X	Y	Z	Dc	X	Y	Z	Dc
Mean	122.3	105.7	50.1	2.16	98.2	104.9	48.7	2.22
Stdev	1.06	1.58	1.54	1.02	1.36	1.48	1.45	0.94

structures obtained from the Schaltenbrand-Wahren atlas superimposed onto the MR slice passing through the centroid of the cloud of points. Our atlas and the Schaltenbrand-Wahren were registered manually to each other using the Voxim software (IVS Solutions AG, Chemnitz, Germany). These figures demonstrate clearly that the final target points chosen intraoperatively cluster around the same anatomic location in the atlas and that the extent of the cluster is smaller than the size of the STN in the transverse images. The spread visible in the sagittal images is caused by the nature of the final stimulator electrode. As opposed to the recording or the marcrostimulation electrode, the final electrode is a four-contact electrode, with the first and last electrodes 7.5 mm apart from each other. Typically, the electrode path is as shown in Fig. 7 and the surgical team tries to place the mid-point of the final electrode at the optimal position determined intraoperatively. But, more than one location along the same path frequently produce a similar response. In these cases the surgical team tries to cover as much as possible of these positions with the fours contacts, which introduces a variability along the electrode path.

To quantify the results shown in Fig. 7, we have computed the position of the centroid for the left and the right clouds of points we have obtained in the atlas. The X, Y, and Z position of the centroid is reported in Table I. We have then computed the distance between each point and its corresponding centroid. This distance, which we call Dc, is also reported in Table I.

B. Creation of an Electrophysiological Atlas

Because the image coordinates of the points at which the signals have been recorded are known, we can extract features from these signals, and map the value of these features onto our atlas. This permits the creation of several atlases, one for each feature. This also permits to compare the usefulness of these features as methods to detect structures of interest. Recall that the boundaries of nuclei and sub-nuclei are not visible in anatomic images but that these boundaries are inferred intraoperatively from micro-electrode recordings (MERs) and responses to stimulations. Our long-term goal is to create an electrophysiological atlas in which these boundaries can be resolved. This will require extracting signal features that are unique to each of the targets of interest. Results we have generated so far indicate that regions that correspond to low and high values for some of these characteristics can be identified in our atlas. Fig. 8 shows the color-coded atlas that corresponds to the spike rate (i.e., number of spikes/second). In this figure, red corresponds to high values, green to low values. To generate this figure, spike rates have been computed for each subject, mapped onto the atlas, and averaged. The optimal target point in the atlas is shown with a small white circle. This figure shows that high values

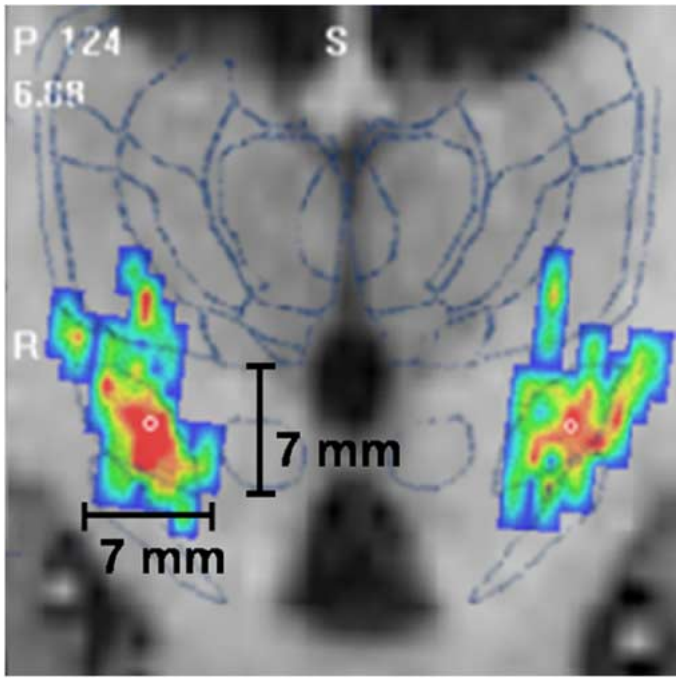

Fig. 8. Map of the mean spike rate projected onto the atlas. Contours that show the structures have been obtained from the Shaltenbrand-Wahren atlas.

for the spike rate correspond to the STN as shown by the contours obtained from the Schaltenbrand-Wahren atlas. One notes a small misalignment of these STN contours and the region of high spike rate on the right side. This is attributed to the difficulty of registering the Schaltenbrand-Wahren atlas with the MR volume.

C. Retrospective Validation of Automatically Selected Target Points

If we define standard target points in the atlas and register the atlas to a new patient, the preoperative target points can be predicted automatically. To evaluate this approach we have used the centroid of the target points mapped onto the atlas as our standard target points and we have mapped those onto the patient image volume to define the preoperative position of the target point. First, we have done this retrospectively on the 21 volumes used to create the atlas. Using a leave-one-out method, we have computed a centroid using 20 volumes and predicted the target point for the 21st volume; the process has been repeated 21 times. To compare the position of the preoperative target point chosen manually using the current clinical procedure and the automatic technique we propose, we define the preoperative placement error. This error is defined as the Euclidean distance between the final intraoperative position selected by the surgical team and the position chosen preoperatively. It is thus the distance by which the surgical team adjusted the position of the electrode during the procedure. Table II reports both the manual and the automatic preoperative placement errors for the 21 subjects used in this study. This table shows that for these patients, the preoperative target point selected automatically is closer to the final target point than the preoperative target point chosen manually, which suggests the possibility of using our approach for the preoperative selection of the target point. We also note that true comparison of the manual and automatic methods is difficult. Indeed, because of its design, the intraoperative platform only permits inserting electrodes along parallel tracks that are separated from each other by 2 mm. If the automatically predicted point falls between tracks, the automatic error includes a term that is perpendicular to the track. Whether or not a track that would have passed through the automatically predicted point would have been better than the one that has been used cannot be assessed retrospectively.

TABLE II

Preoperative Placement Error for STN (in mm)				
	Left		Right	
	Manual	Auto	Manual	Auto
P0	2.59	2.18	4.46	2.53
P1	1.63	2.91	5.02	4.11
P2	1.63	0.90	1.07	0.50
P3		5.53	5.08	
P4	0.00	1.21	5.76	3.36
P5	1.71	1.41	1.65	2.31
P6	3.09	3.19	0.51	1.91
P7	1.03	1.30	2.04	1.48
P8	3.43	3.07	3.27	3.28
P9	4.40	3.27	3.62	2.23
P10	5.19	4.76	5.40	1.35
P11		2.00	3.94	
P12	2.31	1.98	3.65	1.46
P13	0.00	0.71	1.94	2.83
P14	1.45	2.93		
P16	1.58	4.47	4.25	3.05
P17	5.91	3.46	7.34	2.84
P18	5.96	2.37	6.99	2.98
P19	1.96	1.11	0.00	1.74
P20	5.92	5.71	5.00	4.50
Average	2.77	2.61	3.66	2.71
StDev	1.96	1.42	2.14	1.18

D. Prospective Validation of Automatically Selected Target Points

Encouraging results obtained with our retrospective validation method led to a prospective study conducted over a period ranging from March 2004 to June 2004. In this study, our system has been used both to predict targets preoperatively and to provide feedback and guidance intraoperatively. At the beginning of this period, the atlas was frozen and six STN cases involving 12 electrode placements were subsequently performed. The overall procedure involves the following steps: 1) bone markers are implanted; 2) MR and CT images of the patient with the markers are acquired; 3) the procedure is planned; and 4) surgery is performed. Step 3 involves selecting a trajectory (entry and target points) as well as a number of points required for the design of the platform: the anterior and posterior commissure points, one point on the midsagittal plane, and the position and orientation of the markers. Selection of these points is done interactively with the Voxim software. The coordinates of these points are stored on file. This file is then used to manufacture the platform. When ready, the platform

TABLE III

Prospective analysis of automatic prediction of STN (in mm)							
	Automatic targetting			Num of passes		Dist (in mm)	
	Ready	Accepted	Guid.	Auto	Man	Auto	Man
I1	-	-	X	-	2	3.3	4.4
I2	-	-	X	-	2	2.2	3.6
I3	X	X	-	1	-	1.7	
I4	X	X	-	2	-	3.6	
I5	X	X	-	1	-	1.5	2.6
I6	X	X	-	1	-	0.5	
I7	X		-		1	4.2	3.0
I8	X	X	-	1	-	1.5	2.9
I9	-	-	-	-	1	1.8	1.0
I10	-	-	X	-	2	0.5	2.2
I11	-	-	-	-	3	1.9	3.1
I12	-	-	X	-	2	1.2	3.6
Avg.				1.2	1.9	2.0	2.9

is sent to Vanderbilt for the surgery. When our system is used prospectively, we provide at the time of planning (step 3) the neurosurgeon with the target point our system predicts. He then reviews this point and decides whether or not he wants to accept it. Because of logistics problem, we have not always been able to predict the target point on time for planning. In these cases, the plan is done without our predictions but the position at which our system would have placed the target is shown to the surgical team in the OR with our intraoperative system. Table III presents a summary of our experience with our system. In this table, each row corresponds to one implant. "Ready" means that automatically predicted points were available at the time of planning. "Accepted" means that the automatically predicted points were judged acceptable by the neurosurgeon and that they were used to create the StarFix platform. "Guidance" indicates that the automatically predicted points were not available at the time of planning but were available at the time of surgery. They were shown to the surgical team during the procedure. A cross in this column indicates that the surgical team moved, during the surgery, the implant from the manually selected preoperative target toward the automatically predicted target. The number of passes indicates how many passes were required to reach the final target. Under this header, "Auto" means that the automatic target was used for platform design; "Man" means that the manual target was used. The distances are the Euclidean distances between the manual and automatic preoperative targets and the final targets. No entry in the "Man" column under this header means that the surgeon accepted the automatic target and simply did not select one manually.

This table not only shows that the automatically predicted target point is, on average, closer to the final one than the manual target but also, and more importantly, that the number of passes required to reach the target decreases when automatic prediction is used. Out of six times for which our predictions were ready at the time of planning, the final implant was placed four times in one pass on the automatic trajectory. Contrast this with the six cases for which our predictions were not ready on time. Among these, five required a second pass; thus lengthening the procedure and increasing risk to the patient. Among the five manual cases that required more than one pass, the second pass was selected to bring the implant closer to the automatic target three times (cases l1, l2, l10). The last subject (l11 and l12) was a difficult one. The target point was not found on the central track for the right side (l12), which was done first. Another pass was selected to move the electrode in the direction of the automatic target, which was posterior to the manual one. Response to stimulation was poor and a third pass in the posterior-lateral direction was selected. While response was still sub-optimal on this track, it was decided to keep it. On the left side (l11), the final point was not on the central track either. A second pass was selected based on the point selected on the right side. For this case, even though guidance provided by our system was used, it did not lead to the optimal position. However, both for l11 and l12, the automatic target was closer than the manual one to the final target point. In fact, in 7 out of the 9 cases for which we have both manual and automatic targets, the automatic target was closer to the final point (when we do not have both, the surgeon accepted the automatic target without even selecting one manually).

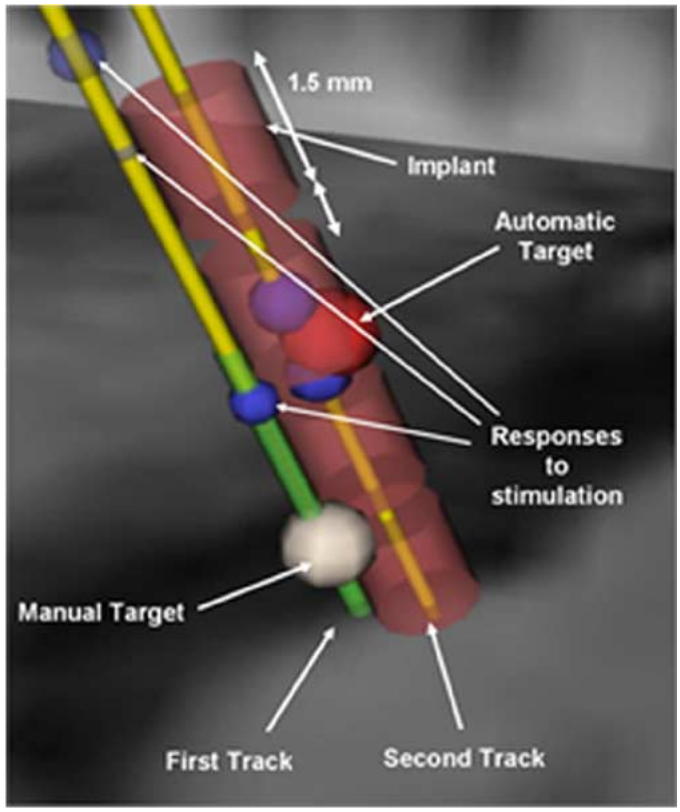

Fig. 9. Portion of the intraoperative display shown to the surgical team.

Fig. 9 illustrates a portion of our intraoperative display as shown to the surgical team during the procedure for patient 5 (l10). The manual target is on the central track (first pass) and shown as a white sphere. Using MER signals, the team has identified the position of the STN along the track (green segment). Stimulation was then performed starting 5 mm higher than the boundary of the STN. Response to stimulation was poor. This is shown as a sphere that is almost transparent on the top left portion of the image (the more transparent the sphere, the poorer the response). A second stimulation a little bit lower shows a

poor response and a small voltage difference between disappearance of symptoms and appearance of side effects (the radius is proportional to this difference). The third stimulation shows a good response but a small voltage difference. The blue sphere labeled "Automatic Target" represents the automatically predicted point. The second track almost goes through it. Stimulation response around the automatically predicted point is good and the final implant (the 4 transparent pink cylinders represent the 4 electrodes) is placed in its proximity.

IV. Discussion and Conclusion

The results presented in this paper indicate that computer-assisted preoperative placement of DBS target points is an achievable goal and that it can be better than a manual approach. For our retrospective study, the automatic method is statistically better than the manual method on the right ($P < 0.05$, one-sided paired t-test) but not on the left. For our prospective study, comparing cases for which we have both a manual and an automatic preoperative target point, the automatic method is statistically better than the manual one ($P < 0.05$, one-sided paired t-test). As stated in Section II-A, T2-weighted images with pulse sequences designed to improve contrast in the STN area were available to the neurosurgeon at the time of planning for the data set used in our prospective evaluation. Despite this, the target of interest could not easily be identified visually, which is consistent with what has been reported by others [4], [17]. This makes manual selection of the targets somewhat subjective and inaccurate even for trained neurosurgeons. Inaccurate preoperative target prediction does in turn complicate and lengthen the surgical procedure. Our study suggests that the computer-assisted method we propose could reduce the duration of the procedure, increase its rate of success, and make it feasible at sites that do not have the expertise that can be found at leading research institutions. Our method could be improved in several ways. It is known that MR images suffer from geometric distortions. Here intraoperative information is acquired in CT coordinates and we register MR and CT images of the same patient using a rigid body transformation. MR images are used to compute the nonrigid registrations required to build our atlas. Geometric distortions in the MR images thus introduce an error. While distortion in T1-weighted SPGR images as the ones we have used are small, they may not be negligible and they may introduce a spread in our clusters. This will be investigated in the future. Fig. 7 shows that some of our final intraoperative target points are mapped outside the STN in the atlas. There are several possible causes for this, ranging from an atypical subject, to poor intraoperative identification of the target point, to mis-registration. One important element that is missing from the current study is information on the outcome of the procedure. It is possible that some of the outliers correspond to patient for which the procedure was not successful in the long term. We are currently collecting outcome information and we will investigate whether or not using this information to build our atlases improves the process. It is also known [18] that the quality of nonrigid registration results depends on the atlas being used. We are in the process of studying the impact of the atlas on the overall process accuracy. Even if perfect preoperative target identification was possible, intraoperative adjustment will likely remain of importance. Because of inaccuracy in the placement of the electrode (limited platform accuracy) or brain motion caused by CSF leak through the burr hole, the electrode may in fact not be placed at the intended position. In these situations, electrophysiological information is critical to adjust the electrode position. Results we have obtained with MER signals indicate that information in these signals can be used to resolve structures that may not be visible in the anatomic images. Our long-term goal is to produce an electrophysiological atlas and to identify signal characteristics that would permit discrimination between structures and substructures. This would be an important component of a system capable of providing real-time feedback to the surgical team. In such a system, signals acquired intraoperatively could be compared to signals stored in our atlas. This would permit the identification of the structures in which the signal is acquired and the computation of intraoperative adjustments.

Acknowledgment

The images and the standard transformations used to validate our rigid body registration algorithm were provided as part of the project: "Retrospective Image Registration Evaluation," National Institutes of Health, Project Number 8R01EB002 124-03, Principal Investigator, J. M. Fitzpatrick, Vanderbilt University, Nashville, TN. The authors would like to thank S. Pallavaram and R. Balachandran for their help with this validation. The authors also thank anonymous reviewers for their constructive comments that have greatly improved earlier versions of this paper [19].

References

[1] G. Deuschl, J. Volkmann, and P. Krack, "Deep brain stimulation for movement disorders," *Movement Disorders*, vol. 17, no. 36(5), pp. S1–S1, 2002.

[2] B. Schrader, W. Hamel, D. Weinert, and H. M. Mehdorn, "Documentation of electrode localization," *Movement Disorders*, vol. 17, suppl. 3, pp. S167–S174, 2002.

[3] P. A. Starr, C. W. Christine, P. V. Theodosopoulos, N. Lindsey, D. Byrd, A. Mosley, and W. J. J. Markers, "Implantation of deep brain stimulators into the subthalamic nucleus: technical approach and magnetic resonance imaging-verified lead locations," *J. Neurosurg.*, vol. 97, pp. 370–387, 2002.

[4] P. A. Starr, "Placement of deep brain stimulators into the subthalamic nucleus or globus pallidus internus: technical approach," *Stereotactic Functional Neurosurg.*, vol. 79, pp. 118–145, 2002.

[5] K. W. Finnis, Y. P. Starreveld, A. G. Parrent, A. F. Sadikot, and T. M. Peters, "Application of a population based electrophysiological database to the planning and guidance of deep brain stereotactic neurosurgery," in *Lecture Notes in Computer Science*. London, U.K.: Springer-Verlag, 2002, vol. 2489, 5th Proc. 5th Int. Conf. MICCAI, pp. 69–76.

[6] K. Finnis, Y. P. Starreveld, A. G. Parrent, A. F. Sadikot, and T. M. Peters, "Three-dimensional database of subcortical electrophysiology for atlas-guided stereotactic functional neurosurgery," *IEEE Trans. Med. Imag.*, vol. 22, no. 11, pp. 93–104, Nov. 2003.

[7] J. M. Fitzpatrick, P. E. Konrad, C. Nickele, E. Cetinkaya, and C. Kao, "Accuracy of customized miniature stereotactic platforms," *Stereotactic Functional Neurosurgery 2005*, vol. 83, no. 1, pp. 25–31, 2005.

[8] E. Cuny, D. Guehl, P. Burbaud, C. Gross, V. Dousset, and A. Rougier, "Lack of agreement between direct magnetic resonance imaging and statistical determination of a subthalamic target: the role of electrophysiological guidance," *J. Neurosurg.*, vol. 97, pp. 591–597, 2002.

[9] R. Li, "Automatic placement of regions of interest in medical images using image registration," Master thesis, Vanderbilt Univ., Dept. Elec. Eng. and Comp. Sci, 2001.

[10] G. K. Rohde, A. Aldroubi, and B. M. Dawant, "The adaptive bases algorithm for intensity based nonrigid image registration," *IEEE Trans. Med. Imag.*, vol. 22, no. 11, pp. 1470–1479, Nov. 2003.

[11] T. B. J. Favre, J. M. Taha, and K. J. Burchiel, "Computer analysis of the tonic, phasic, and kinesthetic activity of pallidal discharges in parkinson patient," *Surg. Neurol.*, vol. 51, pp. 665–673, 1999.

[12] D. L. Donoho, "De-noising by soft-thresholding," *IEEE Trans. Inform. Theory*, vol. 41, no. 3, pp. 613–627, May 1995.

[13] M. Jansen, "Noise reduction by wavelet thresholding," in *Lecture Notes in Statistics*. Berlin, Germany: Springer-Verlag, 2001, pp. 1532–1550.

[14] P. Maragos, J. F. Kaiser, and T. F. Quatieri, "On amplitude and frequency demodulation using energy operators," *IEEE Trans. Signal Process.*, vol. 41, no. 4, pp. 1532–1550, Apr. 1993.

[15] S. Mukhopadhyay and G. C. Ray, "A new interpretation of nonlinear energy operator and its efficacy in spike detection," *IEEE Trans. Biomed. Eng.*, vol. 45, no. 2, pp. 180–187, Feb. 1998.

[16] S. K. Warfield, K. H. Zou, and W. M. Wells, "Simultaneous truth and performance level estimation (staple): an algorithm for the validation of image segmentation," *IEEE Trans. Med. Imag.*, vol. 23, no. 7, pp. 903–921, Jul. 2004.

[17] C. A. Giller, E. E. Babcock, and D. Mendelsohn, "Use of sagittal images of localization of the subthalamic nucleus," *J. Neurosurg.*, vol. 102, pp. 571–575, 2005.

[18] D. Rohlfing, D. B. Russakoff, and J. C. Maurer, "Performance-based classifier combination in atlas-based image segmentation using expectation-maximization parameter estimation," *IEEE Trans. Med. Imag.*, vol. 23, no. 6, pp. 983–994, Jun. 2004.

[19] P. F. D'Haese, E. Cetinkaya, P. E. Konrad, C. Kao, J. M. Fitzpatrick, and B. M. Dawant, "Toward the creation of an electrophysiological atlas for the pre-operative planning and intra-operative guidance of deep brain stimulators (dBs) implantation," in *Lecture Notes in Computer Science*. Berlin, Germany: Springer-Verlag, 2004, vol. 3216, MICCAI, p. 729.